JACS
JOURNAL OF THE AMERICAN CHEMICAL SOCIETY
Article
pubs.acs.org/JACS

Fabrication of 2D Au Nanorings with Pt Framework

Hee-Jeong Jang,[†] Songyi Ham,[†] Jesus A. I. Acapulco, Jr.,[†] Yookyung Song,[†] Soonchang Hong,[†] Kevin L. Shuford,*[,‡] and Sungho Park*[,†]

[†]Department of Chemistry and Department of Energy Science, Sungkyunkwan University, Suwon 440-746, South Korea
[‡]Department of Chemistry and Biochemistry, Baylor University, Waco, Texas 76798, United States

Supporting Information

ABSTRACT: Surface plasmonics of nanomaterials has been one of the main research themes in nanoscience. Spherical and elongated nanoparticles show their corresponding unique optical features mainly depending on the physical dimensions. Here we successfully synthesized Au nanorings having Pt framework (Pt@Au nanorings) with high uniformity through wet-chemistry. The synthetic strategy consisted of serial reactions involving site-selective growth of Pt on the rim of Au nanoplates, subsequent etching of Au nanoplates, followed by regrowth of Au on the Pt rim. In this synthetic method, Au^{3+} ions exhibited dual functionality as an etchant and a metal precursor. The resultant product, Pt@Au nanorings, exhibited unique localized surface plasmon resonance (LSPR) bands originating from the Au shell. The inner Pt skeleton turns out to be important to hold structural stability.

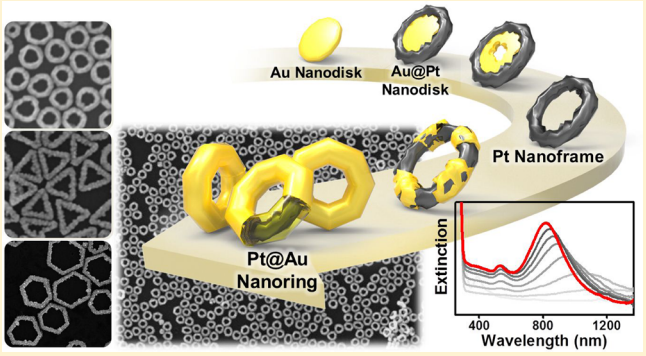

Au nanostructures have unique optical properties depending on their shape,[1] size,[2] dielectric constant,[3] and interparticle gap distance.[4,5] Localized surface plasmon resonance (LSPR) is a unique optical property of Au or Ag metal nanostructures,[6,7] resulting from the collective oscillation of conduction electrons caused by irradiation of electromagnetic fields. Recent research has focused on controlling the shape of Au nanoparticles in order to tune the peak positions of plasmonic bands to fulfill specific purposes. There are many examples for synthesizing a variety of solid Au nanoparticles like spheres,[2] rods,[8] plates,[9] and multipods.[10] These nanoparticles have been designed to tune their interaction with light on their surface, since the change on LSPR allows us to obtain the information related to the surface environment, such as chemical and biological sensing of analytes.

Recently, several synthetic methods have been suggested for the synthesis of hollow metal nanoparticles. In contrast to the analogous solid nanoparticles, hollow nanoparticles are expected to exhibit enhanced interaction with light and surrounding media due to a larger exposed surface than solid nanoparticles. Among the synthetic methods, galvanic replacement reaction[11,12] is the most widely used method for the production of hollow Au nanostructures using Ag nanoparticles and Au precursors. The growth solution for synthesizing colloidal nanoparticles usually contains halide ions, such as Br^- from cetyltrimethylammonium bromide (CTAB), Cl^- from $HAuCl_4$, and I^- from NaI. Binding between Ag^+ ions and halide ions drives down the reduction potential of Ag^+/Ag, favoring the oxidation of Ag^0 by Au^{3+}.[13] This method is not limited to Au, but other noble metals are also applicable through galvanic replacement from initially deposited Ag atoms. When Pt precursors are used instead of Au, the replacement reaction between Ag and $PtCl_6^{2-}$ also results in hollow Pt nanostructures.[14] The final products synthesized from galvanic replacement have hollow interiors and are called nanocages[15,16] and nanoframes.[17] The Xia group[18] investigated a template-engaged replacement reaction between Ag nanocrystals and Au precursors. The reaction involves several steps: the formation of a seamless hollow structure, alloying (Au/Ag), and dealloying steps. However, the large amount of Au precursor often induces fragmentations of the hollow structures during the dealloying process. Using the galvanic replacement reaction, researchers have tried to synthesize size-controllable nanoframes without fragmentation. Formation of initial framework is a critical step before controlling the thickness of nanoframes, since the resultant nanoframes maintain the shape of the initial framework. High site-selectivity of atoms deposited at the edges is also required to avoid the formation of new nucleation site at the terraces for the generation of neat framework. The selective replacement reaction is based on the surface energy difference among the facets[19] and partly driven by passivation of the adsorbed sites by halides and directing agents.

The effort to fabricate metal nanoframes in a controlled manner has led to the evolution of the galvanic replacement reaction into a series of sophisticated reactions including growth and etching. The Kitaev group[20] suggested a growth-etching process for preparing ultrathin Au nanoframes that retained the shape of their original templates. Au was deposited

Received: October 23, 2014
Published: November 20, 2014

dx.doi.org/10.1021/ja510916y | J. Am. Chem. Soc. 2014, 136, 17674−17680

at the edge of Ag nanocrystals under their optimized condition, and the residual inner Ag was etched out by H_2O_2. The etching-growth synthetic method was successfully applied to the synthesis of Pt nanoframes.[21] I_2 selectively etched the edge of Au nanoparticles, which induced selective growth of Pt at the etched site. Further etching of the inner Au nanocrystals finally produced Pt nanoframes.

Colloidal lithography[22,23] is another synthetic strategy for the fabrication of Au nanoframes. This method uses polystyrene spherical particles as a template during deposition of metal by evaporation and as a mask during Ar ion beam etching. However, this method can produce only 2D circular or crescentic structures,[24,25] because it is based on the interface between the substrate and the nanosphere template. In spite of the limitations, many fundamental optical studies on Au nanorings have been progressed, for example, the analysis on LSPR modes[5,22] and measurements of LSPR sensitivity depending on surrounding media.[23,25]

Herein, we synthesized 2D Au nanorings with a Pt skeleton via rim-preferential growth of Pt on Au nanoplates, etching of central Au, and regrowth of Au on Pt framework. Site-selective growth of Pt at the edge of the Au nanoplates played a critical role in securing the final architecture of Au nanoframes during the following Au etching and regrowth steps. In the etching and regrowth step, Au^{3+} ions played dual functions as an etchant and a metal precursor.

The final product, Pt@Au nanorings, exhibited distinguishable LSPR modes from the Au shell on the Pt skeleton. The in-plane LSPR mode could be tuned from the visible region to the near-IR region by changing the size and shape of Pt@Au nanorings. Additionally, for the first time, the out-of-plane LSPR mode could be observed in the nanorings. The proposed synthetic method will provide a platform for the fabrication of various shapes of Pt@Au nanorings.

METHODS

Materials. Hydrogen tetrachloroaurate (III) hydrate ($HAuCl_4 \cdot nH_2O$, 99%) and hydrogen hexachloroplatinate(IV) hydrate ($H_2PtCl_6 \cdot nH_2O$, 99%) were purchased from Kojima. Silver nitrate ($AgNO_3$, 99.8%) was purchased from Junsei. Sodium iodide (NaI, 99.5%) and L-ascorbic acid ($C_6H_8O_6$, 99.5%) were supplied by Sigma-Aldrich. Hydrochloric acid (HCl, 35%) was purchased from Samchun. Cetyltrimethylammonium bromide (CTAB, $C_{19}H_{42}BrN$, 95%) was purchased from Fluka. All chemical materials were dissolved in distilled water (18.2 MΩ). This water was prepared by a Milli-Q water purification system from Millipore.

Preparation of Au@Pt Nanoplate Aqueous Solution. Au nanoprisms[9] were prepared from 5 nm spherical seeds by a three-step, seed-mediated method with iodide ions, as reported previously. Au nanodisks[26] and Au hexagonal nanoplates[27] were synthesized by further procedures with Au triangular nanoplates. All of the Au nanoplate solutions were optically normalized to the same concentration. The synthetic pathway for rim-preferential growth of Pt on Au nanoplates followed the experimental procedure in our previous paper.[28] In the presence of iodide ions (50 μM), 20 mL of 0.05 M CTAB, 5 mL of redispersed Au nanoplates, 30 μL of 2 mM aqueous $AgNO_3$ solution, and 480 μL of 0.1 M aqueous ascorbic acid solution were added to a vial. The mixture was kept at 70 °C. After 1 h, 480 μL of 0.1 M HCl and 300 μL of 2 mM aqueous H_2PtCl_6 solution were added to the mixture with gentle shaking. The mixture was kept at 70 °C for approximately 4 h. After this reaction, the sample was centrifuged, and the supernatant was removed and redispersed in DI water. After washing twice, Au@Pt nanoplates were dispersed into 15 mL of DI water for preparation of stock solution.

Preparation of Pt@Au Nanoring Aqueous Solution. For the preparation of Pt@Au nanorings, Au of Au@Pt nanoplates were etched and regrown. To etch the central Au section of the Au@Pt nanoplates, 2 mL of 0.05 M CTAB with iodide ions (50 μM), 100 μL of 2 mM aqueous $HAuCl_4$ solution and 1 mL of Au@Pt nanoplate stock solution were added to the vial. The mixture was kept at 50 °C for 30 min. Next, 250 μL of 5.3 mM aqueous ascorbic acid solution was added to the mixture, which induced the regrowth of Au on the Pt nanoframes. The mixture was kept at 30 °C for approximately 4 h. The final product included uniformly Au-coated Pt nanoframes, so-called Pt@Au nanorings.

Discrete Dipole Approximation (DDA) Calculation. We have performed DDA calculations for Pt nanoframes, Pt@Au nanorings, and Au nanorings to confirm the interpretation of the experimental spectra. All calculated extinction spectra are for the nanoparticle embedded in a uniform dielectric medium corresponding to water. The spectra presented in the manuscript have been averaged over orientations to represent the optical properties of the particle in solution. The nanoparticle morphologies used in the calculations were based upon the scanning electron microscopy (SEM) images and experimentally determined dimensions. In particular, for Pt nanoframes, the inner diameter was 62 nm, the outer diameter was 106 nm, and the thickness was 23 nm. For the Pt@Au nanorings, the Pt nanoframe was coated by a Au layer (the thickness of 9 nm), making the inner diameter of 45 nm, the outer diameter of 129 nm, and the thickness of 41 nm. For the Au nanorings, the Au nanoring has the same dimension with the Pt@Au nanoring, in which the Pt element in the Pt@Au nanoring was replaced with Au. Ring torus models were used throughout. Custom input files were created that designate particle morphology and material by grid location. A 1 nm dipole spacing was used for all calculations.

Instrumentation. Field emission scanning electron microscopy (FESEM) images were obtained using a JEOL 7100F and a JEOL 7600F. A JEM-2100F was used to acquire transmission electron microscopy (TEM) images. UV−vis−NIR absorption spectra were acquired using UV-3600 (Shimadzu) and S-3100 (Scinco) spectrophotometers. X-ray diffraction (XRD) patterns were obtained using an Ultima IV (Rigaku).

RESULTS

Serial Reactions Involving Etching and Regrowth. As shown in Figure 1, our experimental procedure included the rim-preferential growth of Pt on Au nanoplates, etching of the Au core, and regrowth of Au on Pt framework. The rim-preferential growth of Pt was caused by electron shuttling through thin Ag layers on the Au nanoplates, as mentioned previously.[29] Briefly, the bound Ag^+ ions were reduced to Ag by

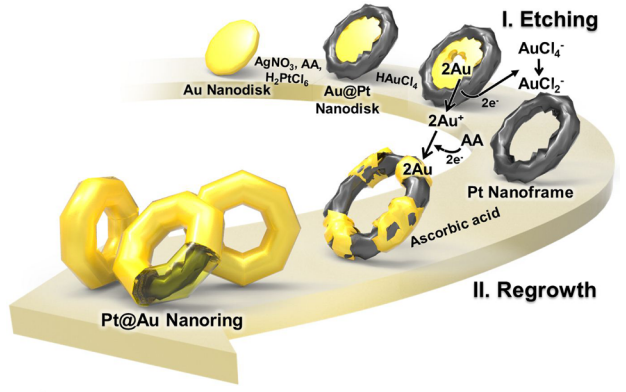

Figure 1. Schematic illustration of the experimental procedures for synthesizing Pt@Au nanorings. Au nanodisks are used as a starting material, and changed into rim-preferentially grown Au@Pt nanodisks via site-selective growth of Pt. The serial reactions for synthesis of Pt@Au nanorings involve (I) etching of central Au part in Au@Pt nanodisks and (II) regrowth of Au on Pt nanoframes.

dx.doi.org/10.1021/ja510916y | J. Am. Chem. Soc. 2014, 136, 17674−17680

a reductant (ascorbic acid). When Pt^{4+} ions are added to this solution, Pt atoms were exclusively reduced at the periphery through the galvanic replacement reaction between Ag and Pt^{4+} ions due to the higher surface energy of the edge and vertex as compared to the terrace. Again, the oxidized Ag^+ ions were reduced to Ag atoms on the Au {111} facets (i.e., the flat top and bottom terraces) by ascorbic acid. Therefore, Ag^+ ions played the role of electron shuttle for Pt^{4+} reduction at the {112} facets (i.e., the edges and vertices). The thickness of Pt rim could be controlled by the total amount of Pt^{4+} ions added to the reaction solution. Next, the central Au nanodisks were selectively etched to Au^+ by the addition of Au^{3+} ions, leaving only the Pt framework. Finally, addition of ascorbic acid to the reaction solution triggered the reduction of Au^+ ions on the surface of the Pt skeleton (regrowth of Au). In the regrowth step, the dissolved Au^+ ions acted as a metal precursor in the reaction solution, and ascorbic acid reduced these Au^+ ions on the surface of the Pt framework.

Similarly, several research groups adopted the serial reactions to combine the galvanic replacement reaction with growth to produce various frame structures with controlling composition and thickness.[13,30,31] The successive process of oxidative dissolution and reductive growth reaction[32] is also similar to our serial reaction, which also contained the dissolution and growth of Au. With iterative oxidative dissolution and reductive growth reactions, one can control seed structural uniformity via the refinement process. In our study, the consecutive process of dissolution and growth was conducted with Au nanoplates having a Pt boundary, resulting in Au nanorings with Pt framework.

In this reaction, Au^{3+} ions played dual functions as an etchant and a metal precursor. The role of Au^{3+} ions as etching agents for Ag nanocrystals is well-known.[33] In the Au@Pt nanoplates, additional $Au^{III}Cl_4^-$ ions were converted to $Au^{I}Cl_2^-$ ions via comproportionation of Au^+, while the central Au atoms are oxidized to Au^+ ions ($AuCl_4^- + 2Au^0 + 2Cl^- \leftrightarrow 3AuCl_2^-$). Comproportionation of $AuCl_2^-$ was originally unfavorable, but the strong binding of $AuCl_4^-$ to CTAB micelles caused the equilibrium constant to increase and resulted in a favorable reaction.[34] This serial reaction conferred significant advantages of not generating unwanted side products or requiring further purification before the regrowth step.

It is noteworthy that aqua regia and KI/I_2 solutions are frequently adopted as Au etchants because both show etching capability. Aqua regia,[29] a solution mixture of nitric acid and hydrochloric acid, has powerful etching ability on Au, but it often causes the aggregation of nanoparticles due to the sudden change of ionic environments. In the case of KI/I_2 mixture, KI improves the solubility of AuI formed by $2Au + I_2 \rightarrow 2AuI$.[35] However, the existence of halide ions strongly affects the growth of nanocrystals because iodide ions strongly bind to metal surfaces. In addition, the excess iodide ions form precipitation in the solution by binding with metal precursors. Therefore, these etchants are not a good choice for the selective etching of the core Au elements in the nanoring synthesis (see Figure S1).

In Figure 2A–C represents the morphology change in each step corresponding to Figure 1, which are rim-preferentially grown Au@Pt nanodisks, Pt nanoframes, and Pt@Au nanorings, respectively. After etching Au in Au@Pt nanodisks by Au^{3+} ions, we observed an empty space in the center of the Pt nanoframes (Figure 2B). The outer diameter of the Pt nanoframes increased from 88 to 106 nm with a Pt rim

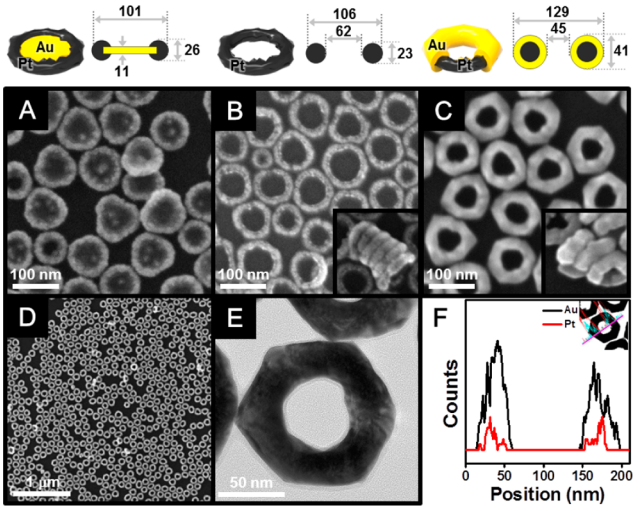

Figure 2. FESEM images of rim-preferentially Pt-coated Au nanodisks (Au@Pt nanodisks) (A), Pt nanoframes (B), Pt@Au nanorings (C). The morphology and dimension information (all scales in nm) are described on the upper side of each image. The insets are their side view (B and C, inset). (D) FESEM image of Pt@Au nanorings with low magnification. (E) TEM image of single Pt@Au nanorings. (F) EDS line mapping of the Pt@Au nanoring in which the red line represents the amount of Pt atoms, and the black line is that of Au atoms. The mapping was conducted along the purple line in inset.

thickness of 23 nm. The Pt nanoframes exhibited a rough surface due to the lattice mismatch between Au and Pt.[36] However, during the Au regrowth step, the Au coating around Pt rims led to smooth Pt@Au nanorings (Figure 2C). Insets in the bottom right corner in panels B and C show the side view of each nanoframe. The thickness at the rim was changed from 26 ± 1 nm (Au@Pt nanodisks), to 23 ± 3 nm (Pt nanoframes), to 41 ± 3 nm (Pt@Au nanorings). The outer diameter of each nanostructure was 101 ± 17, 106 ± 10, and 129 ± 11 nm (detail information on dimension is provided in upper side of each image). Based on the measurements of SEM images, the nanoframes increased by 10 nm in the lateral direction (averaging the difference between the inner and the outer diameters) and by 9 nm in the vertical direction during the growth of Au. This means that Au was grown on the Pt nanoframes almost equally in all directions. The SEM image in panel D shows that the Pt@Au nanorings were prepared with high uniformity without any noticeable byproduct. A zoom-in TEM image in panel E shows the solid rims of Pt@Au nanorings without hollow features. Based on EDS line mapping of Pt@Au nanorings (panel F), we concluded that Pt was located only in the core of the nanoframes, while Au was overcoated on the surface of Pt. The atomic distribution of Au@Pt nanodisks is already confirmed in our previous paper,[28] and that of Pt nanoframes is also provided in Figure S2. The XRD analysis indicated that Pt@Au nanorings exhibited fcc structures of Au (Figure S3).

Assignment of LSPR Bands. The high uniformity of our samples allowed for detailed investigation of the LSPR bands of each sample during the synthetic procedure. We obtained UV–vis–NIR spectra for each sample corresponding to samples in Figure 2A–C and plotted them in Figure 3A. Typically, Au@Pt nanoplates exhibited a broad LSPR band centered at 1062 nm (black trace) due to the surface plasmon coupling between the Au core and Pt rim.[28] Pt nanoframes obtained after etching of central Au showed no features in the vis-NIR spectral window

dx.doi.org/10.1021/ja510916y | J. Am. Chem. Soc. 2014, 136, 17674–17680

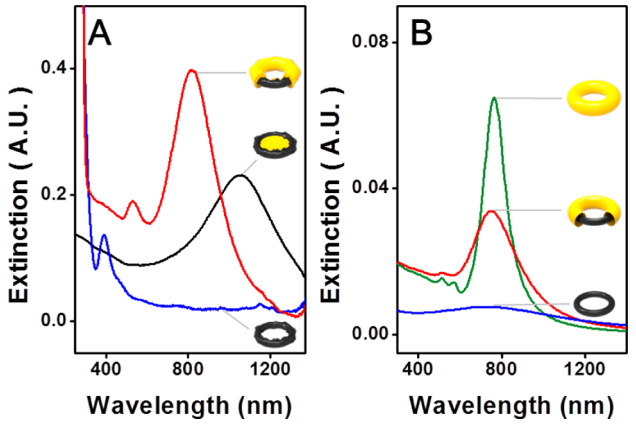

Figure 3. (A) UV−vis−NIR spectra obtained from experimental results with Pt@Au nanorings (red line), Au@Pt nanodisks (black line), and Pt nanoframes (blue line). Each optical spectrum corresponds to the samples shown in SEM images in Figure 2A−2C. (B) UV−vis−NIR spectra obtained from DDA calculation with Au nanorings (green line), Pt@Au nanorings (red line), and Pt nanoframes (blue line).

(blue trace) due to the intrinsic weak surface plasmon activities in the investigated spectral window. The peak at 390 nm originated from the presence of etchant Au^{3+} ions present in the reaction solution. Pt@Au nanorings after regrowth of Au on Pt rims exhibited the dramatic appearance of two distinct peaks that were centered at 530 and 812 nm (red trace). The observed color of the resultant solution is indicated in Figure S4.

In order to assign those peaks, a theoretical calculation based on the discrete dipole approximation (DDA) method was performed, and the resulting spectral profiles were plotted in Figure 3B, showing good agreement with experimental observations. The calculated spectrum of Pt@Au nanorings showed two peaks at wavelengths similar to the experimental results (red trace in Figure 3B). The weak feature at 517 nm corresponded to the out-of-plane dipole mode, and the strong peak at 754 nm was the in-plane dipole mode. In contrast, the pure Pt nanoframes exhibited a very broad feature centered at 729 nm, although the experimental Pt nanoframes showed no feature. Interestingly, the pure Au nanorings (green trace) showed very similar LSPR profiles to the Pt@Au nanorings with an additional peak at 573 nm, which was assigned to the in-plane quadrupole mode (see Figures S5 and S6 for each mode versus E field orientations). In order to observe the weak higher-order modes, effective phase retardation needs to occur. The optical property of thin-layer coated Au on Pt rims was not affected by the presence of the inner Pt. However, the weak feature of in-plane quadrupole mode was completely dampened due to some degree of irregular surface morphology. To the best of our knowledge, this is the first time LSPR bands have been observed for Pt@Au nanorings dispersed in solution.

It is feasible to observe the in-plane mode of Pt@Au nanorings based on the theoretical explanation. According to the hybridization model of plasmon,[37] hollow nanostructures exhibited two plasmons on their inner and outer surfaces, which interacted with one another. This intraparticle surface plasmon coupling caused Pt@Au nanorings to show the in-plane mode. However, the optical spectrum of Pt@Au nanorings displayed only one in-plane mode representing the coupled bonding mode, not the coupled antibonding mode. Since the charge distribution of the bonding mode is a strong dipolar mode which strongly enhanced the field intensity in the nanoring, the bonding mode is preferred.[22]

Real-Time LSPR Band Detection during Serial Reactions. For the further analysis of the synthetic pathways, we monitored the optical spectra with real-time measurements during etching and regrowth steps as shown in Figure 4A and

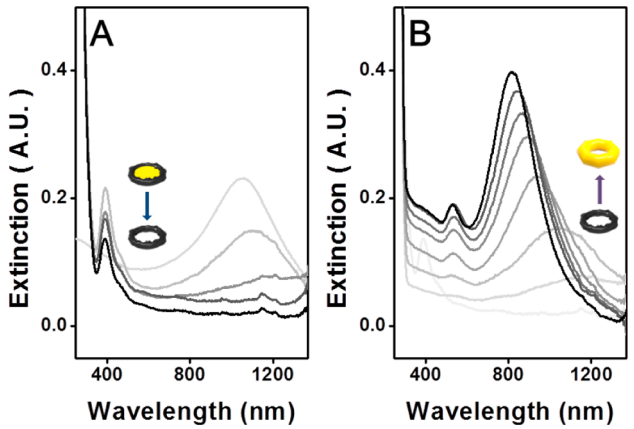

Figure 4. UV−vis−NIR spectra obtained from real-time measurements during the reaction; etching step (A) and regrowth step (B). As the reaction time flows, the spectra are recorded from pale gray to black line. The measurement time is 0, 5, 10, 15, and 20 min during etching and 0, 5, 10, 20, 30, 40 min, 1 h, and 3 h during regrowth.

B, respectively, since the LSPR peaks in the UV−vis−NIR region strongly depend on their shape and structure. The etching process was conducted at 50 °C after adding an aqueous solution of $HAuCl_4$ to the solution containing Au@Pt nanodisks. As shown in Figure 4A, we observed a decrease in the peak intensity at approximately 400 nm due to the consumption of Au^{3+} ions as well as at 1062 nm resulting from the dissolution of the central Au element from the Au@Pt nanodisks. When Au was completely dissolved, there were no noticeable optical features in the vis-NIR spectral region. It is noteworthy that the reduction strength of Au^{3+} ions is not strong enough to induce the dissolution of Pt rims. Then, the addition of ascorbic acid to the reaction environment favors the reduction of Au^{+} to Au in the presence of Pt, leading to the Au overcoating around Pt rim. However, the reduction strength of ascorbic acid is not strong enough to induce the formation of new nucleation, which is critical to the homogeneous coating of Au on Pt rims. The reduction of Au^{+} occurred on the surface of Pt rims, and the resulting product was Pt@Au nanorings without any byproduct. As evident in Figure 4B, two significant changes are observed in a series of spectra during regrowth. First, as the amount of attached Au on the surface of Pt frameworks increased, two LSPR modes appeared at 530 nm (dipole out-of-plane mode) and at 810−1060 nm (dipole in-plane mode). During this regrowth step, the in-plane mode underwent blueshifts of more than 200 nm in wavelength. The blueshifts in peak position might be caused by the decrease in void size and the increase in frame thickness. This tendency is coincident with the results of Au nanorings that were made by colloidal lithography. Other publications have defined the aspect ratio of Au nanorings as the outer diameter divided by the thickness and determined the LSPR shifts based on the aspect ratio.[22,25] During regrowth, the Au coating on the whole surface of the nanorings uniformly thickened, and therefore the

dx.doi.org/10.1021/ja510916y | J. Am. Chem. Soc. 2014, 136, 17674−17680

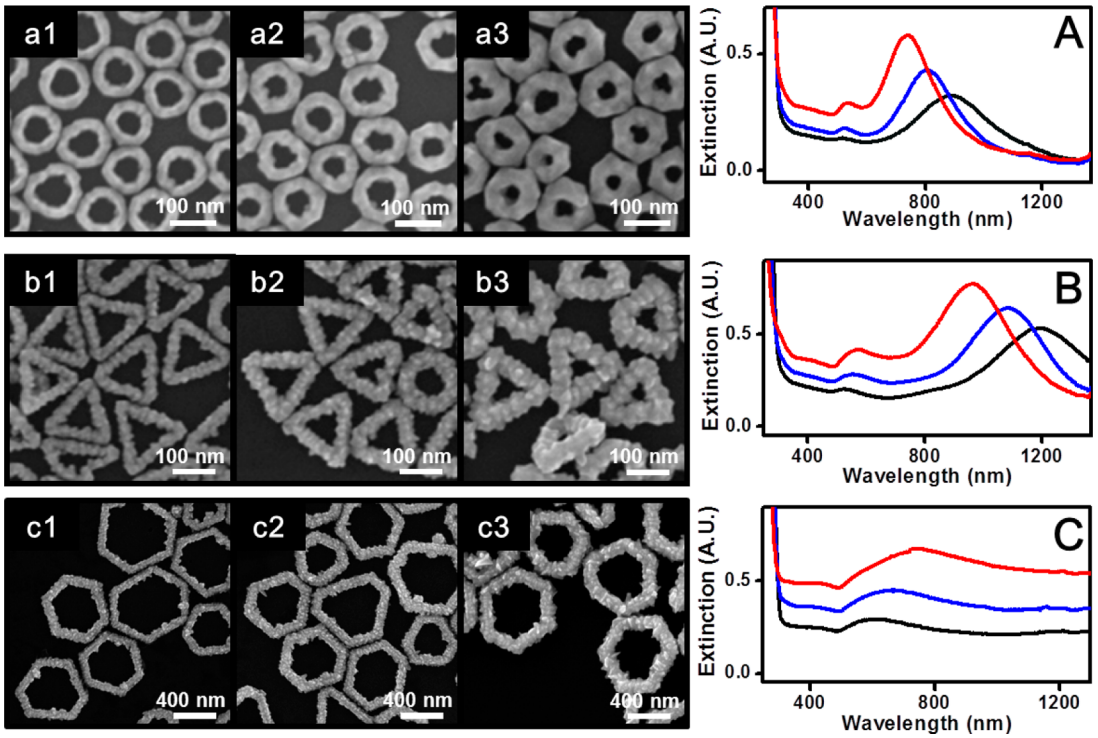

Figure 5. FESEM images of Pt@Au circular nanorings (a1−a3), Pt@Au triangular nanorings (b1−b3), and Pt@Au hexagonal nanorings (c1−c3) depending on the concentration of $HAuCl_4$. 2 mM $HAuCl_4$ aqueous solution is added in reaction solution as the volume of 50, 100, and 200 μL (a1−a3, c1−c3) and 100, 200, and 400 μL (b1−b3). (A−C) UV−vis−NIR spectra are obtained from the samples in SEM images as increasing the amount of Au^{3+} ions (from black, blue, to red line).

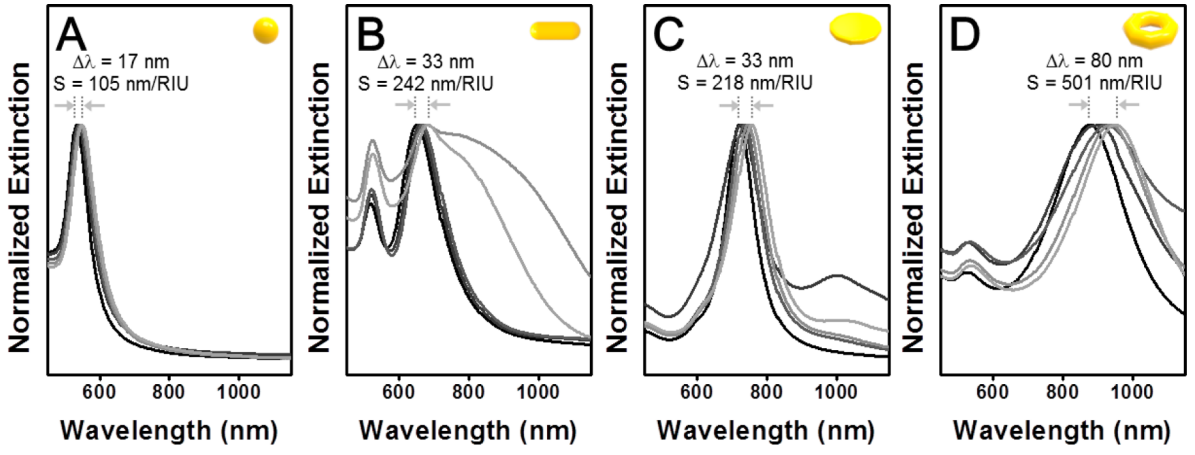

Figure 6. UV−vis−NIR spectra of Au nanospheres (A), Au nanorods (B), Au nanodisks (C), and Pt@Au nanorings (D) depending on the refractive index of solvent. The spectra were measured in H_2O, DMSO, and mixtures of H_2O and DMSO with different ratio. The volume percent of DMSO in H_2O are 0% (black line), 25%, 50%, 75%, and 100% (pale gray line), respectively. Each number above lines indicates the difference on the peak wavelength ($\Delta\lambda$) and the dielectric sensitivity (S).

aspect ratio decreased from 4.6 (Pt framework) to 3.2 (Pt@Au nanoring), which led to the blue-shifts of the in-plane mode. Second, the intensity of both peaks increased as a function of Au thickness. The original spectrum of the optically less-active Pt rim turned into a distinct spectral profile similar to one of pure Au nanorings. The narrow bandwidth of the in-plane mode indicates that the rough surface of Pt rims became smooth by the coating of Au. By monitoring the peak position in the time-dependent spectra, we could fine-tune the thickness of the Au overlayer.

Tunability of LSPR Band in Visible and Near-IR Region. We could tune the plasmonic band of Pt@Au nanorings from visible (700 nm) to near-IR region (1200 nm), as indicated in Figure 5. Our strategy consisted of controlling two factors, the shape of the nanoplate template and the concentration of $HAuCl_4$. This synthetic method could be applied to nanorings of other shapes (i.e., triangular and hexagonal nanorings). To control the shape of the nanorings, (1) the shape of the nanoplate template was changed; circular, triangular, and hexagonal Au nanoplates were used as a starting material. The SEM images and UV−vis−NIR spectra of each nanoplate template are provided in Figure S7. For circular nanorings, the in-plane mode of the plasmonic bands was located along 700−900 nm. In the triangular nanorings, the in-

dx.doi.org/10.1021/ja510916y | J. Am. Chem. Soc. 2014, 136, 17674−17680

plane mode appeared between 900 and 1200 nm. The circular and triangular nanorings had an out-of-plane mode at 530−570 nm. Unlike the other cases, hexagonal nanorings displayed only the out-of-plane mode along 600−800 nm due to their large thickness. (2) The concentration of $HAuCl_4$ could also control the rim thickness of Pt@Au nanoring. As the concentration of Au^{3+} ions in the reaction solution was increased, the thickness of Pt@Au nanorings increased systematically as shown in (a1−a3), (b1−b3), and (c1−c3) in Figure 5.

The difference in the dimension of the nanoplates induced the LSPR bands to shift as indicated in Figure 5A−C. As the concentration of Au^{3+} ions increased (from black, blue, to red line), the rims of Pt@Au nanorings become thicker, and the in-plane mode blueshifted, while the out-of-plane mode was redshifted. We clearly observed the redshifts of out-of-plane mode in the hexagonal nanorings due to the significant change in their thickness, however, the in-plane mode of the hexagonal nanorings was out of the investigated spectral window due to their large dimension.

Sensitivity toward Surrounding Media. In order to analyze the interaction between LSPR bands and the chemical environment surrounding the Pt@Au nanorings, we conducted the measurement of dielectric sensitivity by changing the refractive index of the solvents (Figure 6). A mixture of DI water and dimethyl sulfoxide (DMSO) was chosen for the variation of refractive index solvents. When the volume percent of DMSO was 0% (pure H_2O), 25%, 50%, 75%, and 100% (pure DMSO), the refractive index of the mixed solvent was 1.327, 1.367, 1.408, 1.446, and 1.476 (black line to pale gray line). The increase of refractive index of the solvent strongly redshifted the peak position.[38,39] The wavelength showing maximum extinction caused by LSPR was sensitive to the refractive index, n (or dielectric constant, ε; both are related by $\varepsilon = n^2$).[40] The sensitivity, S, was obtained by calculating the slope of the peak fitting curve in the plot of peak wavelength versus refractive index. Pt@Au nanoring structure indicated the highest sensitivity value in comparisons with solid Au counterparts, such as sphere, rod, and disk (Figure 6 and Table S1). The SEM images of Au nanospheres, nanorods, and nanodisks are provided in Figure S8. The higher sensitivity of the Pt@Au nanorings compared to the Au nanodisks was attributed to larger field enhancement due to the charge distribution of the bonding mode and the electric field distributed to the inside region of the ring structure accessible to the environmental change.[41] The LSPR-sensing ability of Pt@Au nanorings remained that of pure Au nanorings even after inserting the Pt framework inside the ring. Previously, it was theoretically demonstrated that nanorings could serve as effective resonant nanocavities for probing small biomolecules due to the electric field enhancement in the inside of ring cavity.[23] The enhancement factor reached a maximum at the upper and lower ends of the rings. The uniformly enhanced field in the cavity changed sensitively toward the variation of dielectric environment around the nanorings. These observations indicate potential applications in chemical and biological sensors as well as sensitive detection with surface-enhanced Raman spectroscopy in near-IR region.

CONCLUSION

We synthesized Pt@Au nanorings with high uniformity through wet chemistry via site-selective growth of Pt, followed by etching and regrowth of Au. Au^{3+} ions exhibited dual functions as an etchant and a metal precursor. The Au core in the Au@Pt nanoplates was etched out in the form of Au^{+} ions, which were reduced and deposited homogeneously on the Pt nanoframes. The final product, Pt@Au nanorings, exhibited two LSPR bands which were the in-plane and the out-of-plane modes originating from the optically active Au surface. The LSPR bands could be tuned easily by changing the shape of the nanoplate template and the concentration of $HAuCl_4$. The structure of Pt@Au nanorings contributed to the strong enhancement of the interaction between electromagnetic field and chemical environment, resulting in high dielectric sensitivity. In addition, the Pt framework prevented the Pt@Au nanorings from deformation or aggregation that is frequently observed with hollow and thin Au nanoplates. Pt@Au nanorings have potential applications in the fields of biosensing and photothermal treatment by taking advantage of the tunability of LSPR ranges from 700−1200 nm in wavelength as well as high sensitivity due to the open inner space. We will continue to investigate this synthetic pathway for 3D nanocrystals and confirm their structural stability in different chemical and physical environments.

ASSOCIATED CONTENT

Supporting Information

Additional material characterizations. This material is available free of charge via the Internet at http://pubs.acs.org.

AUTHOR INFORMATION

Corresponding Authors

spark72@skku.edu
kevin_shuford@baylor.edu

Notes

The authors declare no competing financial interest.

ACKNOWLEDGMENTS

This work was supported by the Pioneer Research Center Program (2012-0009586). This work was supported by the National Research Foundation of Korea (National Leading Research Lab: 2011-0027911).

REFERENCES

(1) Mock, J. J.; Barbic, M.; Smith, D. R.; Schultz, D. A.; Schultz, S. *J. Chem. Phys.* **2002**, *116*, 6755.
(2) Bastús, N. G.; Comenge, J.; Puntes, V. c. *Langmuir* **2011**, *27*, 11098.
(3) Sönnichsen, C.; Geier, S.; Hecker, N. E.; von Plessen, G.; Feldmann, J.; Ditlbacher, H.; Lamprecht, B.; Krenn, J. R.; Aussenegg, F. R.; Chan, V. Z. H.; Spatz, J. P.; Möller, M. *Appl. Phys. Lett.* **2000**, *77*, 2949.
(4) Haynes, C. L.; McFarland, A. D.; Zhao, L.; Van Duyne, R. P.; Schatz, G. C.; Gunnarsson, L.; Prikulis, J.; Kasemo, B.; Käll, M. *J. Phys. Chem. B* **2003**, *107*, 7337.
(5) Near, R.; Tabor, C.; Duan, J.; Pachter, R.; El-Sayed, M. *Nano Lett.* **2012**, *12*, 2158.
(6) Rycenga, M.; Cobley, C. M.; Zeng, J.; Li, W.; Moran, C. H.; Zhang, Q.; Qin, D.; Xia, Y. *Chem. Rev.* **2011**, *111*, 3669.
(7) Lu, X.; Rycenga, M.; Skrabalak, S. E.; Wiley, B.; Xia, Y. *Annu. Rev. Phys. Chem.* **2009**, *60*, 167.
(8) Jana, N. R.; Gearheart, L.; Murphy, C. J. *Adv. Mater.* **2001**, *13*, 1389.
(9) Millstone, J. E.; Park, S.; Shuford, K. L.; Qin, L.; Schatz, G. C.; Mirkin, C. A. *J. Am. Chem. Soc.* **2005**, *127*, 5312.
(10) Nehl, C. L.; Hafner, J. H. *J. Mater. Chem.* **2008**, *18*, 2415.
(11) Sun, Y.; Mayers, B.; Xia, Y. *Adv. Mater.* **2003**, *15*, 641.
(12) Gonzalez, E.; Arbiol, J.; Puntes, V. F. *Science* **2011**, *334*, 1377.

(13) Métraux, G. S.; Cao, Y. C.; Jin, R.; Mirkin, C. A. *Nano Lett.* **2003**, *3*, 519.
(14) Zhang, W.; Yang, J.; Lu, X. *ACS Nano* **2012**, *6*, 7397.
(15) Skrabalak, S. E.; Au, L.; Li, X.; Xia, Y. *Nat. Protoc.* **2007**, *2*, 2182.
(16) Wang, Y.; Wan, D.; Xie, S.; Xia, X.; Huang, C. Z.; Xia, Y. *ACS Nano* **2013**, *7*, 4586.
(17) Si, G.; Ma, Z.; Li, K.; Shi, W. *Plasmonics* **2011**, *6*, 241.
(18) Sun, Y.; Xia, Y. *J. Am. Chem. Soc.* **2004**, *126*, 3892.
(19) Yin, Y.; Erdonmez, C.; Aloni, S.; Alivisatos, A. P. *J. Am. Chem. Soc.* **2006**, *128*, 12671.
(20) McEachran, M.; Keogh, D.; Pietrobon, B.; Cathcart, N.; Gourevich, I.; Coombs, N.; Kitaev, V. *J. Am. Chem. Soc.* **2011**, *133*, 8066.
(21) Fan, N.; Yang, Y.; Wang, W.; Zhang, L.; Chen, W.; Zou, C.; Huang, S. *ACS Nano* **2012**, *6*, 4072.
(22) Aizpurua, J.; Hanarp, P.; Sutherland, D.; Käll, M.; Bryant, G.; García de Abajo, F. *Phys. Rev. Lett.* **2003**, *90*, 057401.
(23) Larsson, E. M.; Alegret, J.; Käll, M.; Sutherland, D. S. *Nano Lett.* **2007**, *7*, 1256.
(24) Shumaker-Parry, J. S.; Rochholz, H.; Kreiter, M. *Adv. Mater.* **2005**, *17*, 2131.
(25) Bukasov, R.; Shumaker-Parry, J. S. *Nano Lett.* **2007**, *7*, 1113.
(26) Khanal, B. P.; Zubarev, E. R. *J. Am. Chem. Soc.* **2008**, *130*, 12634.
(27) Hong, S.; Shuford, K. L.; Park, S. *Chem. Mater.* **2011**, *23*, 2011.
(28) Jang, H.-J.; Hong, S.; Ham, S.; Shuford, K. L.; Park, S. *Nanoscale* **2014**, *6*, 7339.
(29) Jang, H.-J.; Hong, S.; Park, S. *J. Mater. Chem.* **2012**, *22*, 19792.
(30) Ghosh, T.; Satpati, B.; Senapati, D. *J. Mater. Chem. C* **2014**, *2*, 2439.
(31) Xu, L.; Yin, Z.; Cao, S.-W.; Fan, Z.; Zhang, X.; Zhang, H.; Xue, C. *Chem.—Eur. J.* **2014**, *20*, 2742.
(32) O'Brien, M. N.; Jones, M. R.; Brown, K. A.; Mirkin, C. A. *J. Am. Chem. Soc.* **2014**, *136*, 7603.
(33) Xu, S.; Tang, B.; Zheng, X.; Zhou, J.; An, J.; Ning, X.; Xu, W. *Nanotechnology* **2009**, *20*, 415601.
(34) Rodríguez-Fernández, J.; Pérez-Juste, J.; Mulvaney, P.; Liz-Marzán, L. M. *J. Phys. Chem. B* **2005**, *109*, 14257.
(35) Lee, Y.; Garcia, M. A.; Frey Huls, N. A.; Sun, S. *Angew. Chem., Int. Ed.* **2010**, *49*, 1271.
(36) Fan, F.-R.; Liu, D.-Y.; Wu, Y.-F.; Duan, S.; Xie, Z.-X.; Jiang, Z.-Y.; Tian, Z.-Q. *J. Am. Chem. Soc.* **2008**, *130*, 6949.
(37) Prodan, E. *Science* **2003**, *302*, 419.
(38) Lee, K. S.; El-Sayed, M. A. *J. Phys. Chem. B* **2005**, *109*, 20331.
(39) Link, S.; El-Sayed, M. A.; Mohamed, M. B. *J. Phys. Chem. B* **2005**, *109*, 10531.
(40) Willets, K. A.; Van Duyne, R. P. *Annu. Rev. Phys. Chem.* **2007**, *58*, 267.
(41) Tsai, C.-Y.; Lin, J.-W.; Wu, C.-Y.; Lin, P.-T.; Lu, T.-W.; Lee, P.-T. *Nano Lett.* **2012**, *12*, 1648.